# FINAL TECHNICAL REPORT

NAGW 3127 Fund 23343A

June 1997 Barbara Jones

## Mid-Infrared Observational and Theoretical Studies of Star Formation and Early Solar Systems

The first 2 years of this program were used to make mid-IR observations of regions of star formation in the Orion nebula with the UCSD mid-IR camera at the UCSD/University of Minnesota telescope at Mt. Lemmon. These observations attempted to make the first systematic study of an extended region, known to have newly forming stars, and expected to have complex mid-IR emission. We discovered, to our surprise, that most of the thermal emission originated from extended sources rather than from point sources. This interesting observation made the analysis of the data much more complex, since the chop/nod procedures used at these wavelengths produce a differential measurement of the emission in one region compared to that in the adjacent region. Disentangling complex extended emission in such a situation is very difficult.

In parallel with this work we were also observing comets in the thermal infrared, the other component of the original proposal. Some spectacular data on the comet Swift-Tuttle was acquired and published (Fomenkova, Jones et al., Astron. J., 1995, 110, 1866). This paper describes a changing jet structure observed over a 2 week period. The rotation period of the comet can be measured at 66 hours. The size of the nucleus can also be estimated (at 30 km) from the observed excess flux from the nucleus. These data have lead to the development of models describing the action of dust particles of differing sizes and composition leaving the nucleus. The spatial distribution of the predicted IR emission has been compared to the observed jet structures, leading to estimates of both particles sizes, relative amounts of silicate vs organic grains, and the amounts of dust emitted in the jets vs isotopic emission. This work forms the basis for the PhD thesis of James Sarmecanic.

*Reprinted from:*
THE ASTRONOMICAL JOURNAL VOLUME 110, NUMBER 4 OCTOBER 1995

# MID-INFRARED OBSERVATIONS OF THE NUCLEUS AND DUST OF COMET P/SWIFT-TUTTLE

M. N. FOMENKOVA

B. JONES, R. PINA, R. PUETTER, AND J. SARMECANIC

R. GEHRZ AND T. JONES

# MID-INFRARED OBSERVATIONS OF THE NUCLEUS AND DUST OF COMET P/SWIFT-TUTTLE

M. N. FOMENKOVA

NASA Ames Research Center, MS 239-4, Moffett Field, California 94035-1000 and Center for Astrophysics and Space Sciences, University of California San Diego, La Jolla, California 92093-0011
Electronic mail: mfomenko@ucsd.edu

B. JONES, R. PINA, R. PUETTER, AND J. SARMECANIC

Center for Astrophysics and Space Sciences, University of California San Diego, La Jolla, California 92093-0011

R. GEHRZ AND T. JONES

Astronomy Department, University of Minnesota, 116 Church st. SE, Minneapolis, Minnesota 55455

*Received 1995 January 14; revised 1995 June 21*

## ABSTRACT

We report pre-perihelion observations of comet P/Swift-Tuttle obtained with the UCSD mid-infrared astronomical camera on 12 nights in November 1992. The images were taken through a 1 $\mu$m wide filter centered at 11.65 $\mu$m. During the observing run, the heliocentric distance decreased from 1.13 to 0.98 AU, and the geocentric distance increased from 1.16 to 1.33 AU. The spatial scale of the images was 700–800 km per pixel. In addition, photometric data at wavelengths between 3.6 and 18.5 $\mu$m were obtained on one night. The infrared images cover the cometary activity on time scales from hours to weeks and reveal large changes in the overall morphology of the coma. From periodic changes in the jet patterns we determined the period of nuclear rotation of 67.5±0.4 h. Photometry indicates that the temperature of the coma was 35% higher than the blackbody temperature at the same heliocentric distance and, hence, that the coma was dominated by small particles of average radius of 0.7 $\mu$m. The dust mass loss rate varied with the heliocentric distance as $R^{-6.3}$ and displayed ~40% variation with the rotational phase. Two major jets were present in the images obtained on November 07–17, and a third area became active on November 24–29, increasing the average dust loss rate by a factor of 1.4. The relative positions of the three active areas on the surface of the nucleus are consistent with the positions of the most stable active zones identified by Sekanina [AJ, 86, 1741 (1981)] from the data on the P/Swift-Tuttle apparition in 1862. The radial brightness profiles suggest the radius of the nucleus is 15±3 km. This implies that the nucleus of P/Swift-Tuttle is ~34 times more massive than the nucleus of P/Halley. 

## 1. INTRODUCTION

Studies of the nature and evolution of comets depend crucially on our understanding of the mechanisms and characteristics of cometary activity. During perihelion passage, comets are heated by solar radiation and release gas and dust into the inner solar system, thus forming a coma. From observational studies, combined with extensive modeling, we know that the morphology of the coma is determined not only by the velocity and size distributions and the physical properties of the ejected material, but also by the geometry of jets and sources on the surface of the nucleus, its shape, and rotation geometry with respect to the Sun (review by Sekanina 1990).

Temporal and spatial variations in the distribution of both gas and dust in coma indicate highly anisotropic emission mechanisms which are due to the inhomogeneity of nucleus surface properties and also depend upon the local insolation history. Gas molecules and very small dust grains display semichaotic motion (Horanyi & Mendis 1985), but the motion of the optically efficient micron-sized and larger dust particles is much more collimated and predictable (Kitamura 1987; Rabinowitz 1988). Due to the quasi-coherent behavior of dust particle jet flows, the trajectories can be dynamically extrapolated back to the surface of the nucleus, resulting in location and identification of their sources (Sekanina & Larson 1986). This makes studies of the dust features in the coma an indispensable tool for probing the nature of cometary nuclei.

Imaging of comets in the mid infrared (3–20 $\mu$m) is a very useful method for studying the morphology and the extent of the dust phenomena in the coma. The optical depth in the mid IR is very low ($\sim 10^{-5}$), which facilitates a straightforward interpretation of such images. The 10 $\mu$m wavelength range is dominated by thermal radiation from the dust itself and is sensitive to the dust distribution and its physical properties. A few 10 $\mu$m images of comets have been acquired to date and have demonstrated the importance of this wavelength range for an insight into cometary processes (P/Giacobini-Zinner—Telesco *et al.* 1986; P/Halley—Campins *et al.* 1987; Hayward *et al.* 1987; new comet Wilson—Campins *et al.* 1989; new comet Austin—Fomenkova *et al.* 1993). Analysis of these data has shown that the images are consistent with the premise that the over-

TABLE 1. Observational parameters for Comet P/Swift-Tuttle observations.

| Date (UT) | Airmass | Number of images | R (AU) | Δ (AU) | Elongation (degrees) | Phase Angle (degrees) | Sun-Comet projection angle, North-to-East (degrees) | Linear Resolution (km/pixel) |
|---|---|---|---|---|---|---|---|---|
| 1992 Nov 07.06-07.11 | 1.51-2.04 | 12 | 1.131 | 1.166 | 62.9 | 51.1 | 220.4 | 702 |
| 1992 Nov 08.07-08.11 | 1.58-2.00 | 8 | 1.122 | 1.165 | 62.4 | 51.3 | 221.2 | 701 |
| 1992 Nov 09.09-09.11 | 1.69-1.95 | 4 | 1.114 | 1.167 | 61.9 | 51.5 | 221.9 | 703 |
| 1992 Nov 12.06-12.11 | 1.48-2.05 | 9 | 1.089 | 1.174 | 59.5 | 51.7 | 223.9 | 707 |
| 1992 Nov 13.07-13.11 | 1.54-2.11 | 12 | 1.081 | 1.179 | 59.4 | 51.7 | 224.5 | 710 |
| 1991 Nov 14.06-14.11 | 1.47-2.18 | 14 | 1.073 | 1.184 | 58.7 | 51.7 | 225.1 | 713 |
| 1992 Nov 15.06-15.07 | 1.55-1.59 | 2[a] | 1.066 | 1.190 | 58.1 | 51.6 | 225.7 | 716 |
| 15.08 | 1.66-1.71 | 2[b] | | | | | | |
| 15.09-15.11 | 1.90-2.25 | 6 | | | | | | |
| 1992 Nov 17.05-17.12 | 1.44-2.51 | 18 | 1.052 | 1.205 | 56.7 | 51.5 | 226.8 | 725 |
| 1992 Nov 24.07-24.11 | 1.89-2.63 | 8 | 1.009 | 1.279 | 51.5 | 49.4 | 230.3 | 770 |
| 1992 Nov 26.07-26.11 | 1.80-2.85 | 10 | 0.998 | 1.305 | 49.9 | 48.5 | 231.2 | 786 |
| 1992 Nov 28.05-28.11 | 1.68-3.11 | 15 | 0.989 | 1.334 | 48.3 | 47.4 | 232.1 | 803 |
| 1992 Nov 29.05-29.10 | 1.67-2.77 | 11 | 0.985 | 1.349 | 47.5 | 46.9 | 232.6 | 812 |

a. Taken with a 4.8μ filter.
b. Taken with an 8.7μ filter.

all maximum activity takes place on the sunlit side of a rotating nucleus. In dusty comets with jets, the ejection of dust is restricted to a few discrete active areas representing only a small fraction of the nuclear surface. These areas become dormant when they rotate out of direct sunlight. A temporal lag in sublimation due to thermal inertia also should be taken into account when interpreting the diurnal evolution of the coma.

In this paper we present 11–12 $\mu$m images of comet P/Swift-Tuttle obtained pre-perihelion with the UCSD mid-IR astronomical camera. Comet P/Swift-Tuttle is a very active comet with a period of about 130 yr. It is the parent comet of the prominent Perseid meteor stream (Marsden 1973). Apparitions of this comet in the inner solar system have been traced back to the years AD 188 and 68 BC (Yau *et al.* 1994).

The observing run spanned the time period from 1992 November 7 (IAUC #5654) to November 28 with data taken on 12 nights. We show an extended sequence of high-resolution images revealing the distinctive outlines of prominent features in the morphology of the coma. The temporal evolution of these features is diagnostic of the nuclear rotation. We also discuss how this rotation affects the activity of the comet. For one of these nights, we have photometric data obtained with the University of Minnesota (UM) infrared photometer at the O'Brien 0.76 m telescope. These data are used to derive the temperature of the dust, to estimate the characteristic size of dust grains in the coma, and for comparison with other comets.

## 2. OBSERVATIONS

### 2.1 The Instrumentation

Infrared images of comet P/Swift-Tuttle were obtained with the UCSD mid-IR camera (the "Golden Gopher") on the UCSD/UM 1.5 m telescope at the Mt. Lemmon Observing Facility. The telescope is optimized for observing in the infrared. At 11 $\mu$m, the image spatial resolution is diffraction limited to $\lambda/D \sim 1.5$ arcsec FWHM. The Golden Gopher platescale of 0.83 arcsec/pixel samples the point spread function (PSF) with 2×2 pixels of the array. We used 64 columns×16 rows of the Si:As IBC array, which spanned 53×13 arcsec. On warm nights or when the humidity is high, only a subset of the array can be used since the pixel saturation time due to higher background becomes less than the electronics readout time of 2.7 ms for a full frame. The camera provides good sensitivity in the wavelength range from 5 to 27 $\mu$m. At 11 $\mu$m, the noise equivalent flux density is 40 mJy/arcsec$^2$ in 1 min (including both on and off source time) for a 1 $\mu$m bandwidth. A detailed description of the instrument and observing procedure can be found in Pina *et al.* (1993).

Photometry was carried out with the 15 filter multiaperture infrared GaGe bolometer on the 0.76 m IR telescope of the UM O'Brien Observatory. The bandpasses, calibration, and operational characteristics of the photometer are described by Ney (1974) and Hanner *et al.* (1990). Calibrations for the silicate filters were obtained by interpolating the calibration scales given by Gehrz *et al.* (1974, 1992).

### 2.2 The Infrared Images and Photometric Data

In November 1992, comet P/Swift-Tuttle was imaged at a wavelength of 11–12 $\mu$m during the 12 nights that weather permitted observations. On each night, from 4 to 18 images of the comet were acquired during 1–2 h of observing, the total number of images being 124. Table 1 summarizes the observing parameters and the Sun–comet–Earth geometry. During the observing run, the heliocentric distance $R$ varied from 1.13 to 0.98 AU, and the geocentric distance $\Delta$ varied from 1.17 to 1.35 AU, resulting in a linear resolution at the comet of about 700–800 km/pixel (Table 1) or 840–960 km/arcsec. A typical chop throw between the sky and the object images was 1 arcmin, which was sufficiently large to avoid observable image contamination from a coma flux contribution in the reference beam.

If the dust in the coma is moving with velocity $v_d$, then a

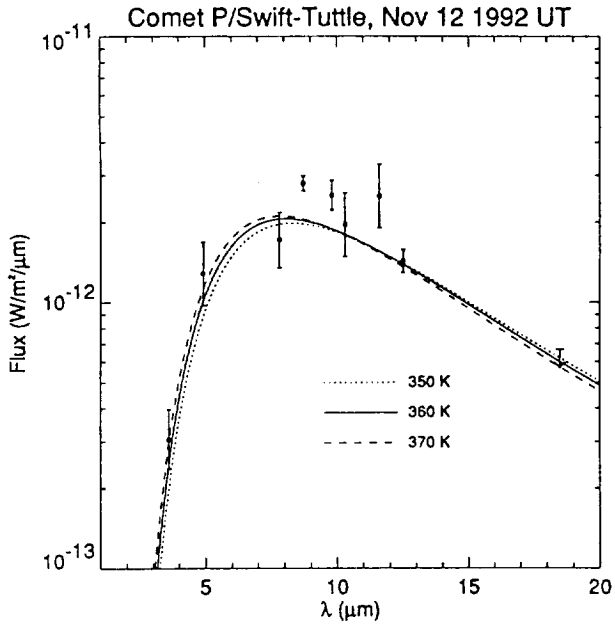


FIG. 2. The 2 to 20 $\mu$m energy distribution of P/Swift-Tuttle. A weak silicate feature is superimposed on a smooth continuum caused by thermal emission of small grains. The fitted blackbody curve yields the grain temperature of 360 K, which is 35% higher than the blackbody temperature at the heliocentric distance of 1.09 AU.

crossing time required for the dust particles to cross the minimal resolution element is:

$$\tau = \varphi\Delta/v_d,$$

where $\varphi$ is an angular resolution and $\Delta$ is the geocentric distance. The crossing time defines an equivalent temporal resolution of the comet emission variability available from the images (Jewitt 1991). The terminal velocity $v_{gas}$ of the gas entraining dust grains into the coma can be estimated from the Bobrovnikov–Delsemme relation (Delsemme 1982):

$$v_{gas}(\text{km/s}) = 0.58R^{-1/2}(\text{AU}), \quad (1)$$

$R$ being the heliocentric distance. Assuming that $v_d/v_{gas} \sim 0.5$–$0.8$ (Finson & Probstein 1968) the temporal resolution is given by (Fomenkova *et al.* 1993):

$$\tau(\text{h}) = 0.70\varphi(\text{arcsec})\Delta(\text{AU})R^{1/2}(\text{AU}). \quad (2)$$

Typical values for comet Swift-Tuttle observations are: $\varphi = 2\times 0.83''$ (two-pixel minimal resolution element), $R = 1$ AU, and $\Delta = 1.2$ AU. The resulting temporal resolution $\tau \sim 1$ h is comparable with the total observing time for each night, but is smaller than characteristic outburst duration of 2–3 h [as estimated by Sekanina (1981) for the previous apparition of P/Swift-Tuttle]. The typical time interval $t_0$ between successive images was 5–10 min, i.e., $t_0 \ll \tau$. Thus, images obtained on the same night were combined together to increase the signal-to-noise ratio and to extend the spatial coverage into the distant parts of the coma (Fig. 1, Plate 101).

The photometric measurements of the IR energy distribution of comet P/Swift-Tuttle were made on 1992 Nov 11.9–12.0 UT through narrowband filters at various wavelengths between 3.6 and 18.5 $\mu$m (Fig. 2), including a number of data points in the silicate emission band at 8–13 $\mu$m. For these measurements, the beam size and chop throw between the source and reference beams were 9 and 45 arcsec, respectively. Corrections, as described by Gehrz & Ney (1992), were made for a coma flux contribution to the reference beam.

### 2.3 Flux Calibrations

For absolute flux calibration, we used the stars $\alpha$ Aql, $\beta$ Peg, and $\alpha$ Tau. Calibrator images were obtained on each night, usually right before and right after the cometary observations. The absolute stellar fluxes were taken from the *IRAS* Point Source Catalog (PSC, 1988) with a quoted uncertainty range of 4%–8% for flux measurement at each wavelength. However, since the satellite data are not color corrected and the *IRAS* bandpasses are much wider than our filter bandpass of 1 $\mu$m, a correction factor needs to be applied. This factor depends on the spectral index of the star in question. The flux densities, $f(\lambda_0)$, quoted in the PSC for $\lambda_0 = 12$, 25, 60, and 100 $\mu$m, were derived assuming an intrinsic spectral index of $-1$:

$$f_q(\lambda)/f_q(\lambda_0) = (\lambda/\lambda_0)^{-1},$$

or

$$F = f_q(\lambda_0)\int f_q(\lambda)/f_q(\lambda_0)R_\lambda\, d\lambda$$

$$= f_q(\lambda_0)\int (\lambda/\lambda_0)^{-1}R_\lambda\, d\lambda,$$

where $F$ is the flux measured by a detector through a given filter, and $R_\lambda$ is the relative filter response (PSC, Table II.C.5). If the actual spectral dependence of flux is $\lambda^{-\beta}$ then

$$F = f(\lambda_0)\int f(\lambda)/f(\lambda_0)R_\lambda\, d\lambda$$

$$= f(\lambda_0)\int (\lambda/\lambda_0)^{-\beta}R_\lambda\, d\lambda,$$

and the actual color-corrected value of the flux density is

$$f(\lambda_0) = f_q(\lambda_0)/K,$$

where the correction factor $K$ equals

$$K = \left[\int (\lambda/\lambda_0)^{-\beta}R_\lambda\, d\lambda\right] \Big/ \left[\int (\lambda/\lambda_0)^{-1}R_\lambda\, d\lambda\right]. \quad (3)$$

This correction has a large effect (up to 50%) and yields the true 12 $\mu$m flux of the star.

For our calibration stars, the spectral index $\beta$ was estimated from the *IRAS* flux values at 12 and 25 $\mu$m, assuming an average error of 6% for each flux measurement:

$$f(12)/f(25) = (12/25)^{-\beta}.$$

*IRAS* spectra of those stars were checked in the *IRAS* Atlas of Low-Resolution Spectra (Olnon *et al.* 1986) to make sure that they are featureless. To obtain true calibration values for our filter centered at 11.65 $\mu$m, we applied an additional small correction (with the same index $\beta$) to the color-corrected flux densities $f(12)$. The resulting fluxes for the

calibration stars are 24.2±1.5 Jy for $\alpha$ Aql, 286.1±23.2 Jy for $\beta$ Peg,[1] and 503.4±31.2 Jy for $\alpha$ Tau.

Overall errors in the flux calibration of the cometary images are due to (i) the intrinsic uncertainties in the *IRAS* measurements, as given above, (ii) sky noise in the calibration star images, and (iii) airmass correction. Fluctuations in the sky emission are essentially random, and, since the raw sky flux is so large, the sky noise is very well described by a Gaussian distribution. Therefore, the uncertainty in the total flux in an aperture containing $N$ pixels is equal to the average sky noise per pixel multiplied by the square root of $N$. On different nights, the sky noise contributes between 5% and 12% to the uncertainty in the raw flux measurement for images of $\alpha$ Aql, and about 1%–3% to the uncertainty in the fluxes of $\beta$ Peg and $\alpha$ Tau. These errors, root-sum-squared with the errors in quoted *IRAS* fluxes given above, yield uncertainties in the flux calibrations between 9% and 15% for $\alpha$ Aql, 7%–11% for $\beta$ Peg, and 5%–8% for $\alpha$ Tau.

To account for the atmospheric extinction, we used an exponential decay approximation of the flux dependence on the airmass. For each night, the calibration coefficients obtained were plotted vs airmass on a log-linear scale. The slope of a linear least-squares fit to these data points yields an extinction coefficient $\alpha$, which, on different nights, ranged from 0.04 to 0.25 mag per airmass. The uncertainties in the best-fit parameters of the airmass correction increase the errors in the flux calibrations. (Usually, either the number of calibration stars was too low or the airmass range covered by them was too narrow to yield a tight fit.) The final uncertainties in the flux calibration of cometary images are between 9% and 18%.

## 3. RESULTS

### *3.1 Overall Morphology and Rotation of the Nucleus*

During its previous apparition in 1862, comet P/Swift-Tuttle was notted for its spectacular activity and was extensively observed [see Sekanina (1981) for the references]. The comet exhibited the dynamical evolution of three types of structures: jets, envelopes, and tail bands, indicating distinctive dust phenomena. Based on drawings and micrometric measurements of the jets made by the 19th century astronomers, Sekanina (1981) derived a nuclear rotation period of 66.5 h and the obliquity of the orbit plane to the equator of 80°, i.e., the rotation axis is almost in the orbit plane. He estimated that no more than 1% of the nucleus surface area was active, located eight discrete emission spots, and inferred a typical ejection duration of ~2–3 h for each of the source regions. Based on orbital calculations, Yau *et al.* (1994) noted a surprising absence of nongravitational perturbations in the P/Swift-Tuttle motion over an interval of more than two millennia. They suggested that either the comet has a very large nucleus, more massive than typical cometary nuclei, or that its emission pattern has been symmetric and extremely stable during this period. We will show later that our data support the notion of a very large nucleus.

[1]The error for $\beta$ Peg is larger because this is an irregular variable with a flux variation of 5% (Hanner 1994).

Our infrared images cover the cometary activity on time scales from hours to weeks. The highly variable night-to-night activity of comet Swift-Tuttle is revealed in the coadded images (Fig. 1). Overall consistency of the images with an approximately 3 d period is immediately seen from the data and was noted by a number of other observers (Jorda *et al.* 1993; Feldman *et al.* 1993). To estimate the rotation period more accurately, we sequenced the images vs rotational phase assuming periods between 50 and 72 h. The most consistent succession of jet development with time (Fig. 3) is reconstructed for a period $T$ of $67<T<68$ h. A period as long as 67 h, or as long as 68 h, changes the sequence in an unacceptable way. Therefore, our best estimate of the period is $T=67.5\pm0.4$ h, which is slightly longer than the average period of 66.5 h derived by Sekanina (1981) from observations of the year 1862.

The sequence of images on Fig. 3 reveals that a drastic change in the activity of P/Swift-Tuttle occurred between Nov 17 and 24. Two dust jets are distinguishable in the cometary images obtained between Nov 07 and 17. The first, strongest jet J1 is apparent in the beginning of the period (Nov 07): contours of constant brightness are elongated westward. It rotates counterclockwise (Nov 13), and dies away in the northwest direction by the middle of the rotation period (Nov 08, 14, 17). In these images the outer contours, determined by the pattern of earlier emission, are elongated to the northwest, but the more recent innermost contours are either circular, or elongated to the southwest. The images of Nov 14 and 17 show that the second, weaker jet J2 becomes active and is directed Sunward. This jet also rotates counterclockwise (Nov 09), and disappears (Nov 12). At the end of the period (Nov 15) jet J1 is awakening again, pointing in the sunward direction.

The pattern of emission from these two major active areas is in good agreement with observations of gaseous species CN, $C_2$, and $C_3$ by Schulz *et al.* (1994) made on three nights in the beginning of October 1992. They estimated that, assuming that the nucleus of P/Swift-Tuttle is in a state of simple rotation, the two active areas producing gas jets are separated by 130° on the surface of the nucleus. From the measurements of dust continuum at 0.483 and 0.523 $\mu$m Schulz *et al.* (1994) also suggested that the gas and dust jets in P/Swift-Tuttle are correlated in some way. Since our observing run took place a month later than theirs, we cannot make a direct comparison of dust and gas emission. In our images, the time interval between the onset of jets J2 and J1 is ~22.5 h, which gives a distance between the active areas of 360°× (22.5 h/67.5 h)≅120°. This result is consistent with the modeling by Sekanina (1981) based on the jet patterns observed during the previous apparition of P/Swift-Tuttle in 1862. He concluded that two most prominent emission areas A and B were separated by 120° in longitude in cometocentric equatorial coordinates. The same areas may be active during the 1992 apparition and responsible for correlated gas and dust production!

But the surface of P/Swift-Tuttle is not frozen permanently in the same, unchanging state. Images of Nov 24, 26, 28, and 29 show the presence of a new, very strong, third jet J3. It is directed southward and has maximum activity in the

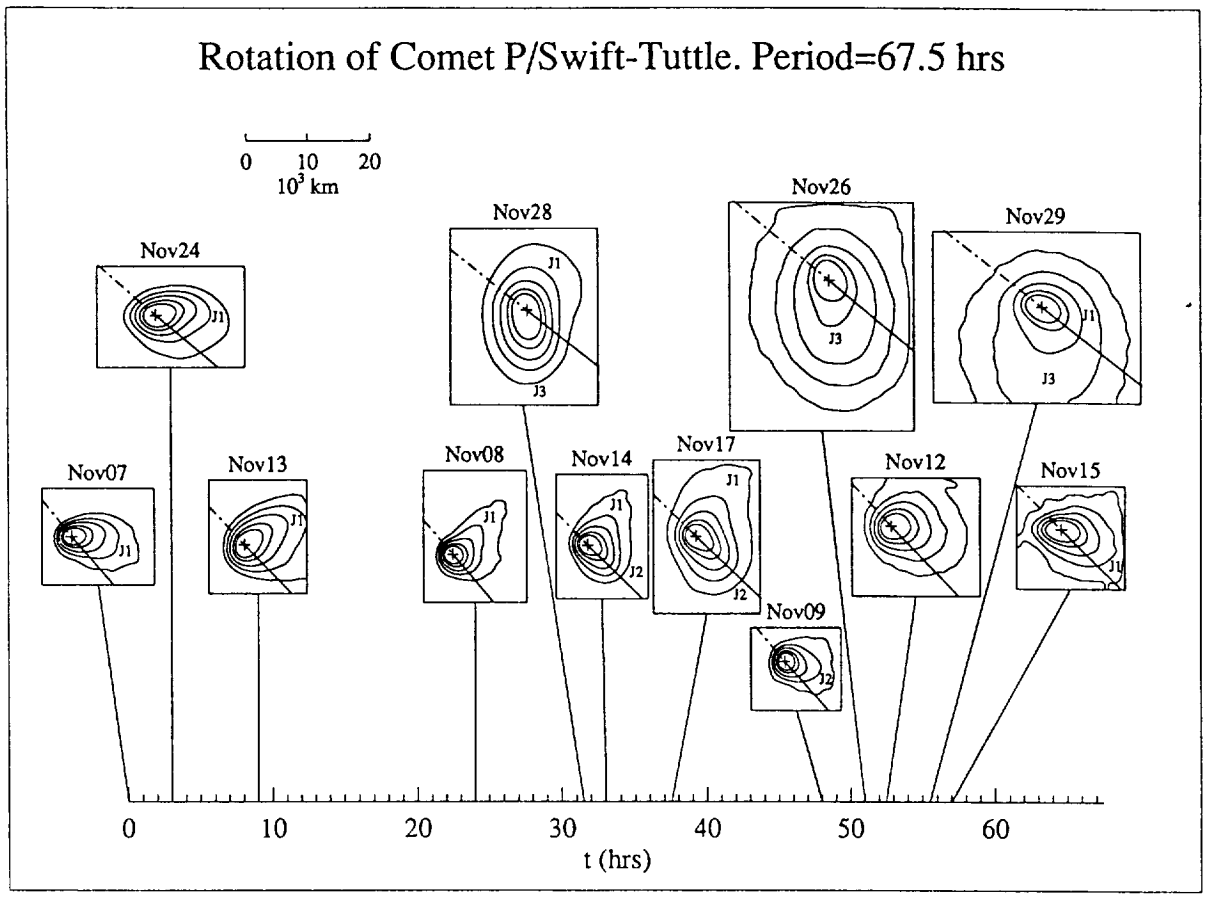


FIG. 3. Images vs rotational phase for a nuclear rotation period of 67.5 h. The brightest pixel of each image is marked by a cross. Contours are drawn at 60%, 40%, 30%, 20%, and 10% level of the peak. The solid line through the brightest pixel of each image shows the sunward direction.

beginning of the last quarter of the period (Nov 26), when it fully obscures the weaker jet J2. Then the activity of jet J3 decreases 5 h later (Nov 29), while jet J1 reappears. The remnants of jet J3 are still seen in the beginning of the period (Nov 24) where outer contours of the coma are slightly elongated southward. The jet J3 is separated from jet J1 by ~29 h in time or by ~155° and may correspond to the active zone C in the model by Sekanina (1981). In 1862, this zone became and stayed active closer to the perihelion than zones A and B.

The sudden activation of a new strong jet indicates that the mechanical and morphological surface properties of P/Swift-Tuttle are heterogeneous and evolve with time. Sekanina (1981) estimated that only about 1% of the surface area of the P/Swift-Tuttle nucleus was active during its 1862 apparition. If the active areas responsible for the jets we observed are indeed the same which were active in 1862, then our observations give evidence of both diurnal and seasonal variations in the activity of the comet. The closer to the perihelion, i.e., to the cometary "summer," the more areas on the surface change from a dormant to an active state. In Sekanina's (1981) model of the 1862 activity of P/Swift-Tuttle, the maximum number of active areas occurs right after the perihelion passage, during the peak of the cometary summer.

Alternatively, if the proximity of angular distances between the three active areas observed in the 1992 and in 1862 apparitions is a random coincidence, this would imply that the upper crust on the surface of the nucleus is unstable and subject to sudden openings of new crevices. Initiation of such a new active area would expose the inner, unmodified volatile-rich fresh material and result in a dramatic increase in the mass loss rate (see further). Fracturing of the surface may be caused by thermal stresses in cometary nuclei due to steep temperature gradients in the surface layer (Tauber & Kuhrt 1987). This explanation is also consistent with the observed jet activation at close heliocentric distance $R<1$ AU.

### *3.2 Photometry and Comparison of Comet P/Swift-Tuttle with Other Comets*

Photometric data obtained on 1992 Nov. 12 were used to estimate the coma temperature (Fig. 2). A blackbody fit to the continuum emission (excluding the silicate band) yields a coma temperature $T_{obs}=360\pm10$ K. The blackbody temperature at a given heliocentric distance $R$ can be determined from the energy balance between the power of absorbed solar radiation and the power emitted by grains in the thermal infrared:

$$\pi a^2 Q_a (L_{Sun}/4\pi R^2) = 4\pi a^2 Q_e \sigma T_{obs}^4,$$

where $Q_a$ and $Q_e$ are the Planck mean absorption and emission coefficients, respectively, $a$ is the average grain radius,

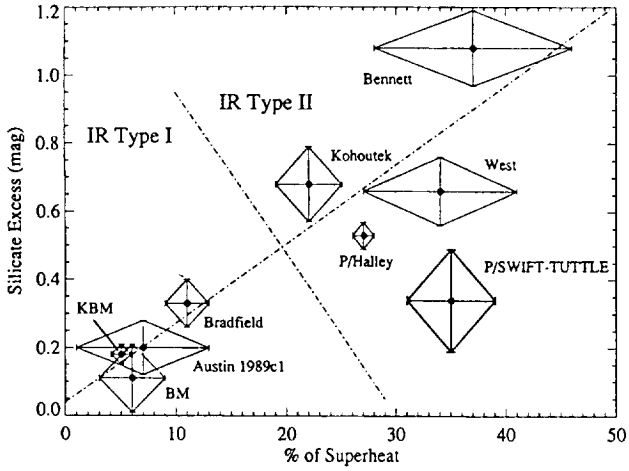


FIG. 4. Comparison of P/Swift-Tuttle with other recent bright comets. The data on superheat and silicate excess in other comets are from Gehrz & Ney (1992).

$L_{Sun}=3.826\times10^{33}$ erg/s is the solar luminosity, and $\sigma=5.6696\times10^{-5}$ erg/cm$^2$/deg$^4$ is the Stefan–Boltzmann constant. Assuming $Q_a=Q_e=1$, the blackbody temperature is

$$T_{bb}\ (\mathrm{K})=(L_{Sun}/16\pi\sigma R^2)^{1/4}=278.3R^{-1/2}\ (\mathrm{AU}). \quad (4)$$

Following Gehrz & Ney (1992), we define the superheat of cometary dust as

$$S=T_{obs}/T_{bb}=(Q_a/Q_e)^{1/4}. \quad (5)$$

For the Nov 12 observations, $R=1.09$ AU, $T_{bb}=267$ K, $S=1.35\pm0.04$, and $Q_e\leq0.3<Q_a$. The high superheat is indicative of small grains present in the coma. If the grains were as large as, or larger than the wavelength of the emitted radiation 10 $\mu$m, then their emissivity $Q_e$ would be close to unity, and their temperature would be close to that of a blackbody [Eq. (4)]. The temperature has to rise above $T_{bb}$ in order for the grains to achieve radiative equilibrium.

The emission in the silicate band (the four points between 8.7 and 11.6 $\mu$m) exceeds the continuum fit by an average of $0.34\pm0.15$ mag. To compare the P/Swift-Tuttle dust component with other comets, we used the data by Gehrz & Ney (1992) (Fig. 4). The observed combination of the superheat and silicate excess characterizes P/Swift-Tuttle as an IR Type II comet.[2] Using calculations by Gilman (1974), as presented in Fig. 5 of Gehrz & Ney (1992), we estimated the average grain size $a\cong0.7\pm0.1$ $\mu$m. This is consistent with P/Swift-Tuttle classification as an IR Type II comet. For comet P/Halley, similar calculations confirmed that, usually, its coma was formed primarily by particles with radii of 0.5–1 $\mu$m.

[2]The classification of comets into IR Type I and II was introduced by Gehrz *et al.* (1989). Type I comets have continuum emission with a low superheat, weak or absent silicate features and Type I (ion) tails. Type II comets have 10 and 20 $\mu$m silicate emission features superimposed on a superheated infrared continuum and prominent Type II (dust) tails. The observed differences between dust emission can be explained by different grain sizes: large (5–10 $\mu$m) particles in comets of IR Type I and small (0.5–1 $\mu$m) particles in comets of IR Type II.

### *3.3 Thermal Infrared Flux and the Mass Loss Rate*

In the steady-state model approximation of cometary dust emission, the dust production rate and the particle velocity do not depend on time, and particles are isotropically emitted from the nucleus. In this case, radial brightness decreases as $1/r$ with the distance from the nucleus. The total thermal infrared flux $F_{IR}$ in a square aperture is roughly proportional to the mass loss rate $M$:

$$F_{IR}=\ln(1+\sqrt{2})(\varphi/\Delta)(3Q_e\sigma T_{obs}^4/4\pi\rho a v_d)M,$$

or (6)

$$F_{IR}(\mathrm{W/m^2})=1.16\times10^{-25}[\varphi(\mathrm{arcsec})/\Delta(\mathrm{AU})]\times[T_{obs}^4(\mathrm{K})/a(\mu\mathrm{m})\rho(\mathrm{g/cm})\times v_d(\mathrm{km/s})]M(\mathrm{kg/s}),$$

where $\varphi$ is the size of a square aperture, $a$ is the average grain size, $\rho$ is the average density, and $Q_e=0.3$. Obviously, comet Swift-Tuttle was not in a steady state as nonisotropic emission, temporal fluctuations in the dust production, and pronounced jets are clearly seen in the images. Many other parameters involved in these calculations are also very uncertain: the actual dust grain size, velocity and density distributions, the dependence of $Q_e$ and $T_{obs}$ on the particle size and composition, etc. Most important is the dependence on the assumed particle size distribution. A considerable amount of the dust mass in the coma is in the form of large particles (>100 $\mu$m, McDonnel *et al.* 1991), which we do not detect in 10 $\mu$m images (Campins *et al.* 1989). Therefore, we can use the steady-state approximation only to obtain a rough measure of the lower limit of the dust mass loss. This estimate allows us a consistent study of short and long term variations in the dust activity of P/Swift-Tuttle during our observing run. Also, the dust production rate of other comets is usually estimated with similar assumptions, which makes the steady-state model a simple, but useful tool for comparing the productivity of different comets.

The total thermal flux $F_{IR}$ can be estimated from our measurements of the flux $f_{11}$ in a 1 $\mu$m wide filter centered on 11.65 $\mu$m as

$$F_{IR}=f_{11}\sigma T_{obs}^4\ \Big/\left[\int_{11.15}^{12.15}B_{bb}(\lambda,T_{obs})d\lambda\right], \quad (7)$$

where $\lambda$ is the wavelength in $\mu$m, and $B_{bb}(\lambda,T_{obs})$ is the Planck energy distribution. Assuming that on all dates the superheat of the cometary dust was the same as on Nov 12 (i.e., the temperature of the grains was 35% higher than the blackbody temperature at the same heliocentric distance: $T_{obs}=375.7\ R^{-1/2}$), we find that $F_{IR}\cong16.26\ f_{11}$. The mass loss rate shown in Figs. 5(a) and 5(b) was calculated from (6) for $a=0.7$ $\mu$m, $\rho=1.0$ g/cm, $v_d=0.46R^{-1/2}$, and $Q_e=0.3$.

Dust production in Fig. 5(a) varies approximately as $R^{-6.3}$, which agrees very well with the heliocentric dependence of the water production rate as derived by Hoban *et al.* (1993) from a vast set of independent observations. This heliocentric dependence is much steeper than a typical for comets $R^{-2}$–$R^{-4}$ one (Gehrz & Ney 1992). The increment of the mass loss rate at $R<1$ AU is caused by the activation of

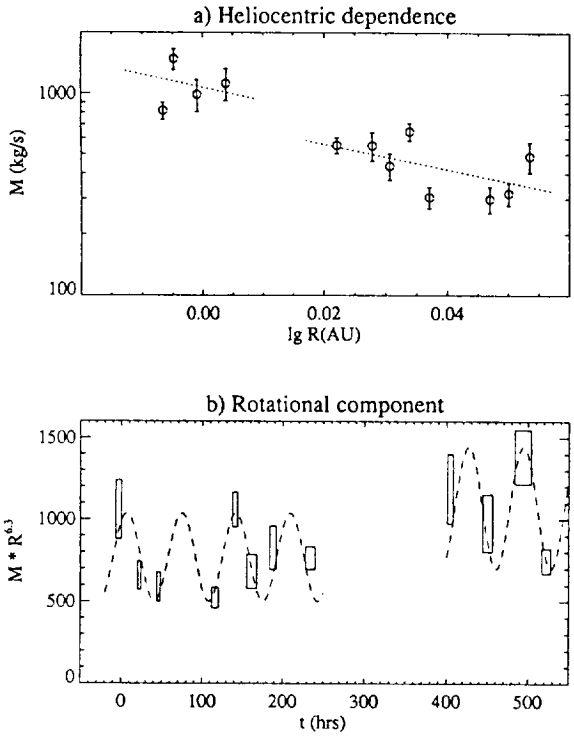


FIG. 5. Dust mass loss rate of P/Swift-Tuttle. (a) Heliocentric dependence. The heliocentric distance was decreasing with time. The dotted line is the least squares approximation showing the $R^{-6.3}$ dependence of the dust mass loss rate. (b) Rotational phase dependence. The sinusoidal curve is used as the simplest periodic function. The width of each box is determined by the angular size of the corresponding image as follows from Eq. (2): the mass loss rate obtained from our measurements is an average over this time interval. The height of each box shows the error of measurement.

jet J3 during the week between November 17 and 24 (cf. Sec. 3.1). Emission from the new area increased the average activity by a factor of 1.4. The overall activity is comparable with that of P/Halley ($\geq 10^3$ kg/s at $R=1$ AU) and is about an order of magnitude higher than in other comets (Gehrz & Ney 1992).

Day-to-day fluctuations in the mass loss rate [Fig. 5(b)] are roughly consistent with the suggested rotation period of 67.5 h. On November 7–17, the dust production achieved maximum when the jet J1 was active, and dropped to the minimum during the intervals of the jet J2 activity. The difference between maximum and minimum dust production is ~40%, and similar variation in the water production was found from *IUE* observations (Feldman *et al.* 1993). The data presented by Schulz *et al.* (1994) show the following day-to-day abundance variations of gaseous species: 25% for CN, 26% for $C_2$, and 40% for $C_3$. This quantitative agreement confirms the hypothesis that, in contrast to comet P/Halley, the gas and dust jets in comet P/Swift-Tuttle are correlated. Remarkably, Feldman *et al.* observed a clear maximum in the water production on Nov 4. That is one rotation period earlier than our first observation of Nov 7, and, in accordance with the rotational dependence presented in Fig. 5(b), activity peaks at this rotational phase.

### *3.4 The Size of the Nucleus*

Sudden activation of strong jets evidently contradicts the suggestion of a uniquely stable and symmetric pattern of emission of P/Swift-Tuttle made by Yau *et al.* (1994). Sekanina (1981) also inferred from his model calculations that different areas had been active during different rotations of the nucleus, the total number of active areas being up to eight. We consider the alternative hypothesis by Yau *et al.* (1994): that a surprising absence of nongravitational perturbations in the orbital motion of this comet is due to a very large nucleus.

High-resolution infrared imaging gives us a key to direct observations of cometary nuclei even for highly active, Halley-type comets near perihelion. Consider an ideal "unit" comet producing $M=10^3$ kg/s of dust[3] in 1 $\mu$m size particles of the density $\rho=1$ g/cm$^3$ at $R=\Delta=1$ AU. In accordance with Eq. (1), the velocity of dust grains is $v_d=0.5$ km/s, and, with a superheat of 1.35, the temperature of grains is 376 K. From Eq. (6) we estimate that the infrared flux of such a comet observed in a 1 arcsec square aperture equals: $I=4.6\times10^{-12}$ W/m$^2$.

Suppose that the nucleus of the unit comet has an average radius $x$ km (with a corresponding surface area of $4\pi x^2$ km$^2$) and radiates as a point source at a blackbody temperature $T_{bb}=278$ K. The resulting infrared flux is given by

$$C=\sigma T_{bb}^4 (x/\Delta)^2,$$

or

$$C(\mathrm{W/m^2})=2.534\times10^{-24} T_{bb}^4(\mathrm{K}) x^2(\mathrm{km}). \quad (8)$$

For $x=10$ km, $C$ equals to $1.5\times10^{-12}$ W/m$^2$, implying that the contribution from the nucleus to the central brightest pixel is at least comparable with the flux from the dust. Note that the smaller the size of the central pixel (that is the higher the angular resolution), the larger is the relative contribution of the nucleus flux.

In real images, however, the point source flux becomes spread out over some finite area described by the point spread function (PSF) of the instrument. Approximating our PSF with a Gaussian radial profile, $\mathrm{PSF}=(1/2\pi\delta^2)\exp(-r^2/2\delta^2)$, the contribution of the point source flux to the central pixel is reduced and given by

$$C_{\mathrm{PSF}} \leq C/2\pi\,\delta^2,$$

where $\delta$ is determined by the full-width half maximum (FWHM) of the PSF as

$$\delta^2=\mathrm{FWHM}^2/8\ \ln 2$$

for a Gaussian approximation of the PSF. Computer modeling was applied to convolve the sum of the $1/r$ dust contribution and the point source contribution from the nucleus with the instrumental PSF. The FWHM was estimated for each night from the calibration star images. The ratio of the nuclear flux $C$ to the dust flux in the central pixel was used as a free parameter in the model. Values of $C$ obtained from the best fit between the model and experimental radial brightness profiles yield an average nucleus radius of $x=(15\pm3)$ km. This result is consistent with photometric measure-

[3]This value of $M$ is close to the average mass loss rate in P/Halley at 1 AU and is about an order of magnitude higher than in most comets (Gehrz & Ney 1992).

ments by Williams who suggested that P/Swift-Tuttle nucleus should be at least 24 km across [reported in News Notes, Sky and Telescope 89(1), 1995, page 13]. For comparison, the dimensions of the elongated comet P/Halley nucleus are (15.3×7.2×7.22) km, thus giving an average radius of 4.8 km (Szego 1991).

We estimate that for the same density, the nucleus of P/Swift-Tuttle would be ~34 times more massive than the nucleus of P/Halley. Hughes & McBride (1989) showed that the mass of a meteor stream is proportional to the mass of its parent comet multiplied by its dust-to-gas mass ratio. The mass of the meteor stream Perseid associated with P/Swift-Tuttle is $(46\pm5)\times10^{12}$ kg and the average mass of the meteor stream Orionid/Eta Aquarid associated with P/Halley is $(1.5\pm0.4)\times10^{12}$ kg (Jenniskens 1994). Assuming the same dust-to-gas mass ratio in P/Halley and P/Swift-Tuttle, the ratio of masses of their meteor streams is 31, which is in excellent agreement with our result.

## 4. SUMMARY

Comet P/Swift-Tuttle at the heliocentric distance of 1 AU was one of the most active periodic comets after P/Halley and it demonstrated "Halley-type" behavior in some other respects too. Both P/Halley and P/Swift-Tuttle are old evolved comets having retrograde orbits (inclination >90°). Their comae are dominated by small (~1 $\mu$m) particles. Images of both comets were consistent with the presence of anisotropic flows of ejecta emanating from discrete active regions (vents) on the rotating cometary nucleus. Moreover, it was suggested that the same vents have remained active since their previous apparitions in 1910 for P/Halley (Rabinowitz 1988) and in 1862 for P/Swift-Tuttle (Schulz *et al.* 1994; this work). This hypothesis, if true, implies a certain degree of stability and, hence, might be used to infer the physical strength of the upper crust on the nuclei of old evolved periodic comets. Future missions landing on the surface of a cometary nucleus would shed more light on this problem.

The activity of individual vents seems to remain stable from one apparition to another, but responds to the diurnal cycle and is affected by seasonal variations. To be fully addressed in the future, it requires a long series of observations of a comet which would provide comprehensive information on day-to-day temporal evolution of cometary activity pre- and post-perihelion. Our observations of P/Swift-Tuttle, as well as the interpretation of the 1862 observations by Sekanina (1981), show that the number of active areas tends to increase closer to perihelion. In our case, there were two sources of jets on November 07–17, and the third vent became active in the images on November 24–29. The mass loss rate depended on the heliocentric distance as $R^{-6.3}$. The initiation of strong emission from the new area increased the average mass loss rate by a factor of 1.4. From periodic changes in the jet pattern we determined the rotation period of P/Swift-Tuttle of 67.5±0.4 h. The dust production varied by ~40% with rotational phase.

In contrast to P/Halley, the dust and gas jets appear to be correlated in P/Swift-Tuttle. Observations of both comets give rise to speculations about possible heterogeneity of their nuclei (Mumma *et al.* 1990; Fomenkova & Chang 1993; Hoban *et al.* 1993), but there is not enough data to draw more certain conclusions.

The radial brightness profiles calculated for the mid-infrared images of P/Swift-Tuttle are consistent with the presence of a large nucleus, which contributes a non-negligible thermal infrared flux to the central part of each image. We estimated the radius of the nucleus to be 15±3 km. If the densities of the two nuclei are equal, the nucleus of P/Swift-Tuttle is ~34 times more massive than the nucleus of P/Halley. This may provide an explanation of the absence of nongravitational perturbations in the motion of comet P/Swift-Tuttle.

We suggest that the differences in the general morphology of comae of new and old comets combined with the differences in the dust grain size distributions may be the principal physical parameters correlated with the dynamical age of comets. For example, images of dynamically new comet Austin (1989c1=1990V) obtained with the same UCSD camera did not reveal significant dust structures in the morphology of the coma, although the resolution was higher, <300 km per pixel (Fomenkova *et al.* 1993). Either the dust emission was more or less uniform from the whole nucleus (with a slight prevalence on the sunlit side), or the dust grains were ejected in a large number of microjets indistinguishable as separate events from ground-based observations. The long history of apparitions in the inner solar system causes formation of a thick dusty mantle, possibly glued together by complex nonvolatile organics, on most of the surface of a comet (Brin & Mendis 1979). Such an impenetrable crust constraints the activity to a few active areas which are, probably, crevices reaching deeper volatile-rich layers. It effectively decreases and may be even completely prevents the dust emission from the rest of the surface. This scenario implies that the particle size distributions may be different in old and new comets. The coma of new comet Austin was dominated by larger particles (10 $\mu$m) with the size distribution $f(a)\sim a^{-1}$ (Lisse 1992), while the coma of P/Halley contained a larger fraction of small particles (0.5–1 $\mu$m) with the size distribution $f(a)\sim a^{-3.7}$ (McDonnell *et al.* 1991). The photometric measurements of P/Swift-Tuttle indicate that the average size of dust grains in its coma is ~0.7 $\mu$m. A detailed modeling of dust emission processes in P/Swift-Tuttle to determine better its grain size distribution is a subject of our future work.

M. N. Fomenkova acknowledges the support of California Space Institute and thanks the National Research Council for a Resident Research Associateship at NASA Ames Research Center. B.J. and J.S. were supported under NASA Grant NGW-3127 from the Origin of Solar System Program. Partial support for R.P. was provided by NASA Graduate Student Fellowship. We thank Dr. P. Blanco for kindly providing his image processing routines. Comments by D. Cruickshank and by the reviewer S. Larson helped us to improve the manuscript.

REFERENCES


Brin, G. D., & Mendis, D. A. 1979, ApJ, 229, 402
Campins, H., Telesco, C. M., Decher, R., & Ramsey, B. D. 1987, A&A, 187, 601
Campins, H., Lien, D., Decher, R., Telesco, C., & Clifton, K. 1989, Icarus, 80, 289
Delsemme, A. H. 1982, in Comets, edited by L. L. Wilkening (University of Arizona, Tucson), pp. 85–130
Finson, M. L., & Probstein, R. F. 1968, ApJ, 154, 327
Feldman, P. D., McPhate, J., A'Hearn, M. F., McFadden, L. A., & Haken, M. E. 1993, in Asteroids, Comets, Meteors (abstr.), IAU Symposium No. 160, 106
Fomenkova, M. N., & Chang, S. 1993, in Lunar Planet. Sci. Conf., 24, 501
Fomenkova, M. N., Jones, B., Pina, P., Puetter, R. C., McFadden, L. A., Abney, F., & Gehrz, R. D. 1993, Icarus, 106, 489
Gehrz, R. D., & Ney, E. P. 1992, Icarus, 100, 162
Gehrz, R. D., Hackwell, J. A., & Jones, T. W. 1974, ApJ, 191, 675
Gehrz, R. D., Ney, E. P., Piscatelli, J., Rosenthal, E. & Tokunaga, A. T. 1989, Icarus, 80, 280
Gehrz, R. D., Grasdalen, G. L., & Hackwell, J. A. 1992, in Encyclopedia of Physical Science & Technology, 2, 125
Gilman, R. C. 1974, ApJS, 28, 397
Hanner, M. S. 1994, private communication
Hanner, M. S., Newburn, R. L., Gehrz, R. D., Harrison, T., Ney, E. P., & Hayward, T. L. 1990, ApJ, 348, 312
Hayward, T. L., Gehrz, R. D., & Grasdalen, G. L. 1987, Nature, 326, 55
Hoban, S., Reuter, D., DiSanti, M., & Mumma, M. 1993, Icarus, 105, 548
Horanyi, M., & Mendis, D. A. 1985, ApJ, 294, 357
Hughes, D. W., & McBride, N. 1989, MNRAS, 240, 73
IRAS Point Source Catalog, NASA RP-1190, 1988
Jenniskens, P. 1994, A&A, 287, 990
Jewitt, D. C. 1991, in Comets in the Post-Halley Era, edited by R. L. Newburn, M. Neugebauer, and J. Rahe (Kluwer, Dordrecht), pp. 19–65
Jorda, L., Colas, F., & Lecacheux, J. 1993, in Asteroids, Comets, Meteors (abstr.), IAU Symposium No. 160, 150
Kitamura, Y. 1987, Icarus, 72, 555
Lisse, C. M. 1992, Ph. D. thesis, University of Maryland
Marsden, B. G. 1973, AJ, 78, 654
McDonnel, J. A. M., Lamy, P. L., & Pankiewicz 1991, in Comets in the Post-Halley Era, edited by R. L. Newburn, M. Neugebauer, and J. Rahe (Kluwer, Dordrecht), pp. 1043–1074
Mumma, M., Reuter D., & Magee-Sauer K. 1990, BAAS, 22, 1088
Ney, E. P. 1974, ApJ, 189, L141
Olnon, F. M., Raimond, E., & IRAS Science Team 1986, IRAS Atlas of Low-Resolution Spectra, A&AS, 65, 607
Pina, R. K., Jones, B., & Puetter, R. C. 1993, in Infrared Detectors and Instrumentation, SPIE Proc., 1946, 66
Rabinowitz, D. L. 1988, A&A, 200, 225
Schulz, R., McFadden, L. A., Chamberlin, A. B., A'Hearn, M. F., & Schleicher, D. G. 1994, Icarus, 109, 145
Sekanina, Z. 1981, AJ, 86, 1741
Sekanina, Z. 1990, AJ, 100, 1293
Sekanina, Z., & Larson, S. 1986, AJ, 89, 1408; AJ, 92, 462
Szego, K. 1991, in Comets in the Post-Halley Era, edited by R. L. Newburn, M. Neugebauer, and J. Rahe (Kluwer, Dordrecht), pp. 713–732
Tauber, F., & Kuhrt, E. 1987, Icarus, 69, 83
Telesco, C. M., *et al.* 1986, ApJ, 310, L61
Yau, K., Yeomans, D., & Weissman, P. 1994, MNRAS, 266, 305

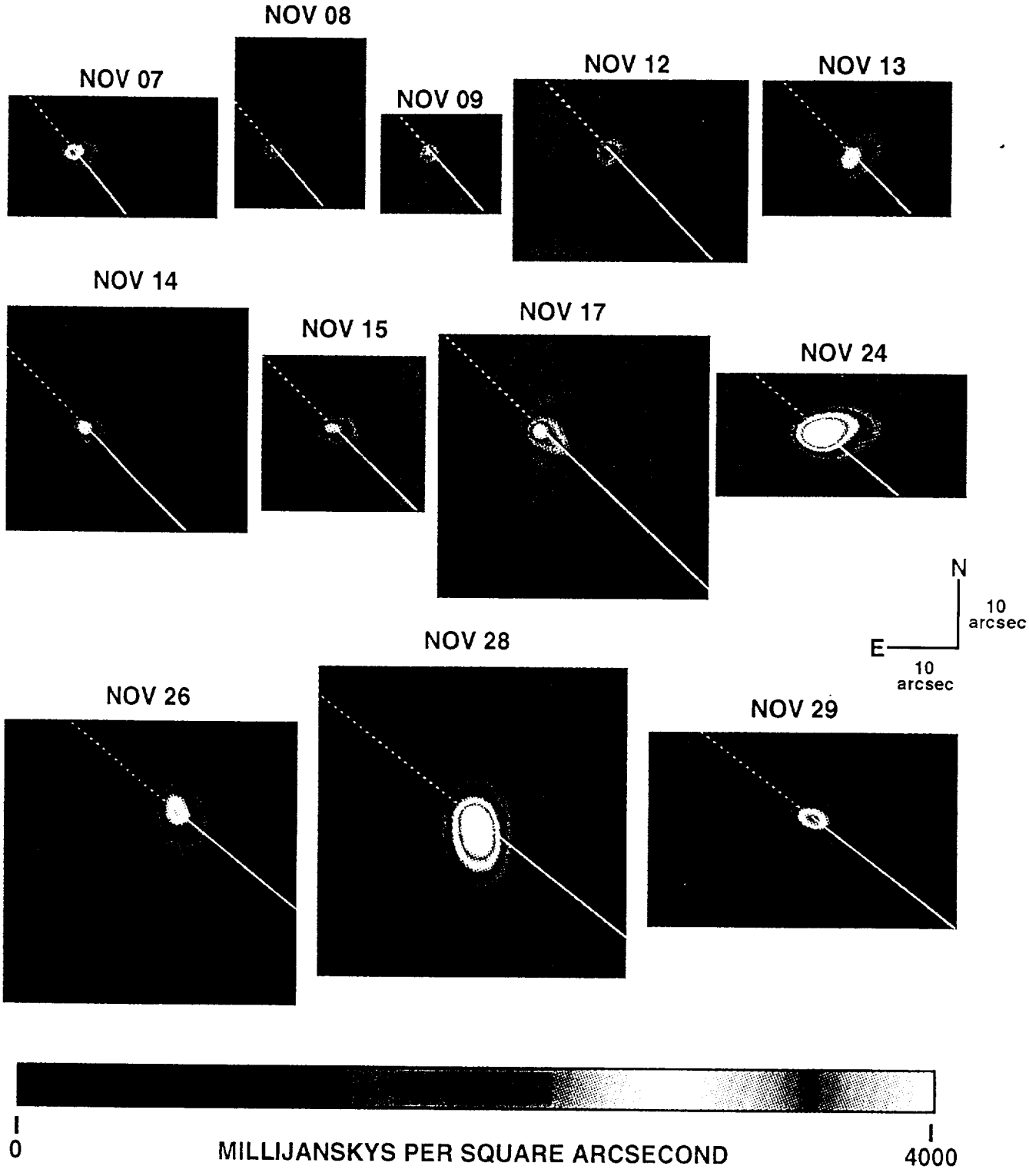


FIG. 1. Coadded thermal infrared images of comet P/Swift-Tuttle. North is upward, and east is leftward. The solid line through the brightest pixel of each image shows the Sunward direction.